

Soft-X-Ray Spectroscopy of the Amine Group: Hydrogen Bond Motifs in Alkylamine/Alkylammonium Acid-Base Pairs

Maria Ekimova¹, Markus Kubin², Miguel Ochmann³, Jan Ludwig², Nils Huse³, Philippe Wernet^{2,*}, Michael Odelius^{4,*}, Erik T. J. Nibbering^{1,*}

¹*Max Born Institute for Nonlinear Optics and Short Pulse Spectroscopy, Max Born Str. 2A, 12489 Berlin, Germany.*

²*Institute for Methods and Instrumentation for Synchrotron Radiation Research, Helmholtz-Zentrum Berlin für Materialien und Energie GmbH, Albert-Einstein-Strasse 15, 12489 Berlin, Germany.*

³*Institute for Nanostructure and Solid State Physics, Center for Free-Electron Laser Science, Luruper Chaussee 149, 22761 Hamburg, Germany.*

⁴*Department of Physics, Stockholm University, AlbaNova University Center, 106 91 Stockholm, Sweden.*

Email: nibberin@mbi-berlin.de ; odelius@fysik.su.se ; wernet@helmholtz-berlin.de

Abstract

We use N K-edge absorption spectroscopy to explore the electronic structure of the amine group, one of the most prototypical chemical functionalities playing a key role in acid-base chemistry, electron donor-acceptor interactions and nucleophilic substitution reactions. In this study we focus on aliphatic amines and make use of the nitrogen 1s core electron excitations to elucidate the roles of N-H σ^* , and N-C σ^* contributions in the unoccupied orbitals. We have measured N K-edge absorption spectra of the ethylamine bases $\text{Et}_x\text{NH}_{3-x}$ ($x=0..3$; Et- = C_2H_5^-) and the conjugate positively charged ethylammonium cation acids $\text{Et}_y\text{NH}_{4-y}^+$ ($y=0..4$; ; Et- = C_2H_5^-), dissolved in the protic solvents ethanol and water. Upon consecutive exchange of N-H for ethyl-groups we observe a spectral shift, a systematic decrease of the N K-edge pre-edge peak and a major contribution in the post-edge region for the ethylamine series. Instead for the ethylammonium ions, the consecutive exchange of N-H for ethyl-groups leads to an apparent reduction of pre-edge and post-edge intensities relative to the main-edge band, without significant frequency shifts. Building on findings from our previously reported study on aqueous ammonia and ammonium ions, we can rationalize these observations by comparing calculated N K-edge absorption spectra of free and hydrogen bonded clusters. Hydrogen bonding interactions lead only to minor spectral effects in the ethylamine series, but have a large impact in the ethylammonium ion series. Visualization of the unoccupied molecular orbitals shows the consecutive change in molecular orbital character from N-H σ^* to N-C σ^* in these alkylamine/alkylammonium ion series. This can act as benchmark for future studies on chemically more involved amine compounds.

1. Introduction

Alkylamines R_xNH_{3-x} ($x = 0..3$) are nitrogen-containing compounds having a pyramidal geometry, with a specific number of N-H bonds that can vary between three and zero and a related number of alkyl-groups (varying between zero and three), plus a lone electron pair at the N atom. The lone pair can accept an additional proton, connecting the alkylamines bases to the respective conjugate alkylammonium $R_yNH_{4-y}^+$ ($y = 0..4$) ionic acids, that have tetrahedral coordination around the nitrogen atom (see Figure 1). Ammonia (R_xNH_{3-x} ($x = 0$)) and the ammonium ion $R_yNH_{4-y}^+$ ($y = 0$) are the smallest in this series. When prepared in solution, however, they are not necessarily the simplest in these series since hydrogen bonding to solvent molecules as well as between themselves (at high concentration) can have a strong and symmetry-breaking influence. Amines play a key role in biological systems, as functional groups in proteins, or as messenger molecules (neurotransmitters) in living species. Amines can act as nucleophilic agents in substitution (S_N1 , S_N2) reactions, most notably the Mannich reaction.^{1, 2} Determination of the electronic structure of the amine group allows for a better understanding of its chemical reactivity.³ Within the series of amines or alkylamines a consecutive exchange of N-H with alkyl-groups causes a reduction in the number of possible N-H interactions within reaction pairs and with the surrounding solvent. It also leads to changes in the electron-density of the central nitrogen atom due to the electron-inductive effect of alkyl-groups. Together with steric hindrance factors of the alkyl-groups, the electronic induction of alkyl-groups govern the capacity of the amino-group as reducing agent in electron donor-acceptor interactions, as well as a proton-accepting site in acid-base chemistry. Related to the electronic properties of the amino-group is its capability of hydrogen bond formation of alkylamines and alkylammonium compounds

(Figure 1), where the N-H hydrogen bond donating and N lone pair hydrogen bond accepting interactions change in the series, directly connected to the systematic changes in proton affinity (that are typically characterized in solution phase through the respective pK_a -values).

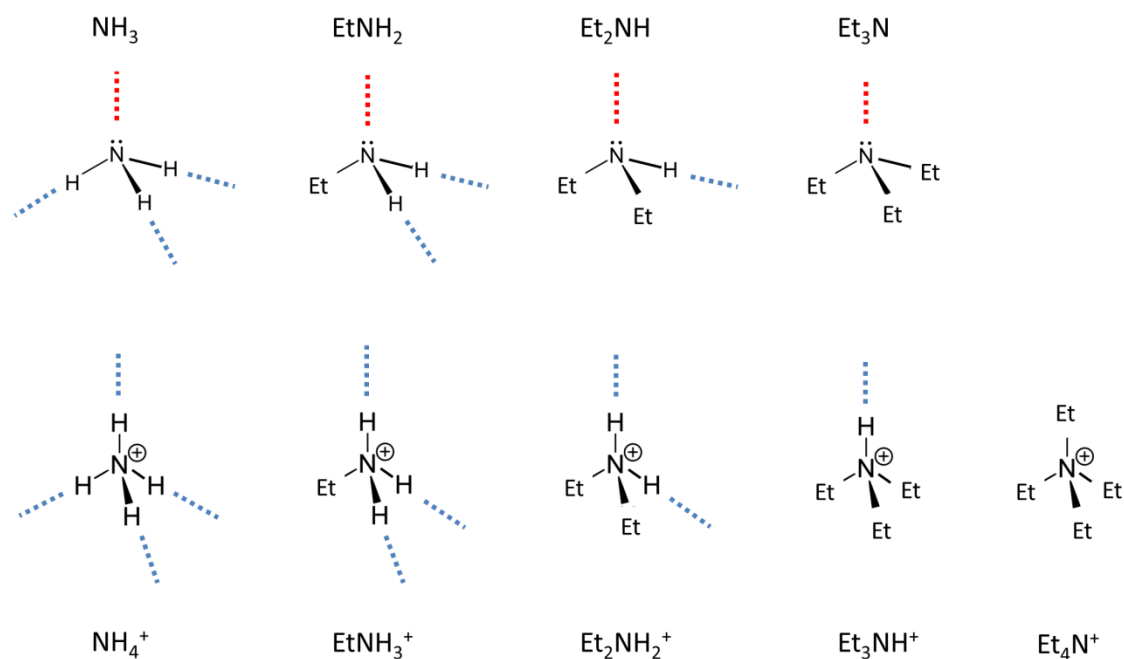


Figure 1 Geometries of the pyramidal ethylamine bases $\text{Et}_x\text{NH}_{3-x}$ ($x=0..3$; Et- = C_2H_5^-) and the conjugate tetrahedral positively charged ethylammonium cation acids $\text{Et}_y\text{NH}_{4-y}^+$ ($y=0..4$; ; Et- = C_2H_5^-), with possible hydrogen bonding donating (blue) or accepting (red) interactions with solvent molecules.

Reports on the electronic structure of amines and conjugate protonated ammonium compounds deduced from soft-x-ray spectra are scarce, ranging from the benchmark ammonia/ammonium ion system,^{4, 5} to amino acids,^{6, 7, 8, 9, 10, 11} aromatic amines,^{12, 13, 14} ionic liquids¹⁵ and nucleic acid bases.¹⁶ Among the soft x-ray spectroscopic methods suited for studying amines and ammonium compounds, N K-edge x-ray absorption spectroscopy (XAS) is particularly powerful in addressing intra- and intermolecular N-H interactions as it directly

accesses the unoccupied N-H orbitals. The impact of hydrogen bonding interactions, protonation and electron donor-acceptor interactions of N-H groups and their relative importance for the pre-, main- and post-edge transitions in the N K-edge XAS spectrum in terms of possible changes in transition frequencies and intensities, and the role of particular alkyl or aromatic functionalities in the soft-x-ray spectra remain rather unexplored. In this paper we present results obtained on the N K-edge absorption spectra of the ethylamines R_xNH_{3-x} ($x = 1..3$; $R = C_2H_5^-$, abbreviated as Et-), measured in ethanol, and the conjugate ethylammonium ions $R_yNH_{4-y}^+$ ($y = 1..4$; $R = C_2H_5^-$, abbreviated as Et-), measured in water. We use N K-edge XAS in transmission mode, using a transmission flatjet¹⁷ to probe the N 1s core electronic excitations to unoccupied molecular orbitals with varying N-H and/or N-C σ^* antibonding character. This systematic investigation of the electronic sensitivity to ligand substitution and hydrogen bonding builds on and extends from our previously published results on ammonia and the ammonium ion in water.⁵

2. Methods

Chemicals. Ethanol was purchased from Merck (Uvasol for the spectroscopy). The solutes ethylamine (Sigma-Aldrich, 66.0-72.0 % in H₂O), diethylamine (Sigma-Aldrich, ≥ 99.5 %), triethylamine (Fluka, ≥ 99.5 %), ammonium chloride (AnalaR Bio, NORMAPUR, 99%), ethylamine hydrochloride (Sigma-Aldrich, ≥ 98.0 %), diethylamine hydrochloride (Sigma-Aldrich, ≥ 99.0 %), triethylamine hydrochloride (Sigma-Aldrich, ≥ 99.0 %) and tetraethylammonium chloride (Sigma-Aldrich, ≥ 98.0 %) were used without further purification. Aqueous ammonia solutions were prepared by dilution of 26 % w/w NH₃*H₂O

(Merck, for analysis EMSURE). Concentrations used were ranging between 0.2 – 0.5 M. All samples were filtered and degassed before each XAS measurement.

XAS spectra. The N K-edge absorption spectra were recorded in transmission mode using a set up based on a novel liquid flat jet technique described in detail previously.¹⁷ In short, two laminar single jets obliquely collide under an angle of 48° leading to a flatjet formation consisting of two consecutive sheets. The first sheet has the form of a leaf bound by a thick rim. An ordinary HPLC (High Performance Liquid Chromatography) pump was used to pump a liquid through the 50 µm nozzles with a flow rate of about 3.20 ml/min. The liquid was later collected and frozen in a cold trap. The thickness of the film at the measurement point was varied in the 2.0-3.0 µm range to achieve sufficient signal.

XAS experiments were performed at the UE52-SGM beamline at the synchrotron radiation source BESSY II at the Helmholtz-Zentrum Berlin.¹⁸ BESSY II was operated in multi-bunch mode resulting from top-up injection of the electron storage ring. The monochromator exit slit was set to 100 µm, resulting in a bandwidth of ~110 meV (Gaussian FWHM) at 390 eV. The X-ray beam diameter on the sample was nominally 60*60 µm. The x-ray flux incident on the sample was on the order of 10¹¹-10¹² photons/s. The x-ray radiation transmitted through the sample was detected by a GaAs photodiode (Hamamatsu, G1127-04). Every sample scan was corrected for signal contributions of the beamline and the solvent (both were measured under the same conditions as the sample solutions). To calibrate the energy scale for our absorption measurements we have used the ammonia spectrum published before⁵ as a reference since it had previously been calibrated in incident energy using the nitrogen gas spectrum also recorded during that particular previous beamtime.

Computations. For analysis of the experimental data, theoretical XAS spectra based on density functional theory (DFT) were derived for R_xNH_{3-x} ($x=0..3$) and $R_yNH_{4-y}^+$ ($y = 0..4$), in both isolated and hydrogen bonded configurations. The DFT calculations were performed in the CP2K software suite (version 5.0)^{19, 20, 21, 22} using a dispersion corrected BLYP functional^{23, 24, 25, 26} and a cubic simulation cell of dimension 30 Ångström in combination with a Poisson solver to model isolated systems.²⁷ The molecules and clusters were geometry optimized with the Gaussian and Plane Wave (GPW) method,¹⁹ in which we used GTH pseudo-potentials^{28, 29, 30} in combination with Gaussian basis sets (TZVP-GTH)³¹ to describe the Kohn-Sham orbitals and an auxiliary plane wave basis (with a cut-off of 300 Ry) to describe the electron density. The simulated x-ray absorption spectra were derived from full core-hole excited (XFH) transition potential self-consistent field (SCF) calculations³² as implemented in the Gaussian augmented plane wave (GAPW) method,³³ using an all-electron description with the 6-311++G(2d,2p) basis set^{34, 35} and a 600 Ry cut-off for the plane wave expansion of the electron density. Each discrete XAS spectrum was based on 200 unoccupied Kohn-Sham orbitals in the XFH SCF. The discrete transitions were convoluted with a Gaussian broadening with a full-width half-maximum of 0.4 eV and all simulated spectra were shifted by -10.05 eV for direct comparison to the measured spectra.

3. Experimental Results

We display in Figure 2 (left column) our experimental N K-edge absorption spectra of the alkylamine compounds R_xNH_{3-x} ($R= C_2H_5-$ (Et-); $x=0..3$), measured in ethanol. Clearly the pre-edge feature, observed at 401.2 eV for NH_3 , shifts towards higher frequency, and appears to be merging with the main edge band for Et_2NH . To emphasize the changes in spectral features upon consecutive exchange of N-H for N-Et groups, the spectrum of $Et_{(x-1)}NH_{3-(x-1)}$ ($x=1..3$) is shown as grey line in the panel for each alkylamine Et_xNH_{3-x} ($x=1..3$). A pronounced absorption at frequencies higher than 403 eV is already present for $EtNH_2$, i.e. when only one N-H group is exchanged with an N-ethyl-group. In the series, we see that this broad and pronounced post-edge feature is clearly associated with the presence of ethyl-groups in the molecules. This suggests a different type of underlying transition than those ascribed to the post-edge of $NH_3(aq)$.^{4, 5} Moreover, despite similarities in pre- and main-edge frequency positions for the alkylamines, the step-wise change in the character of the unoccupied orbitals as the consecutive exchange of N-H for ethyl-groups is expected to be manifested in the N K-edge XAS.

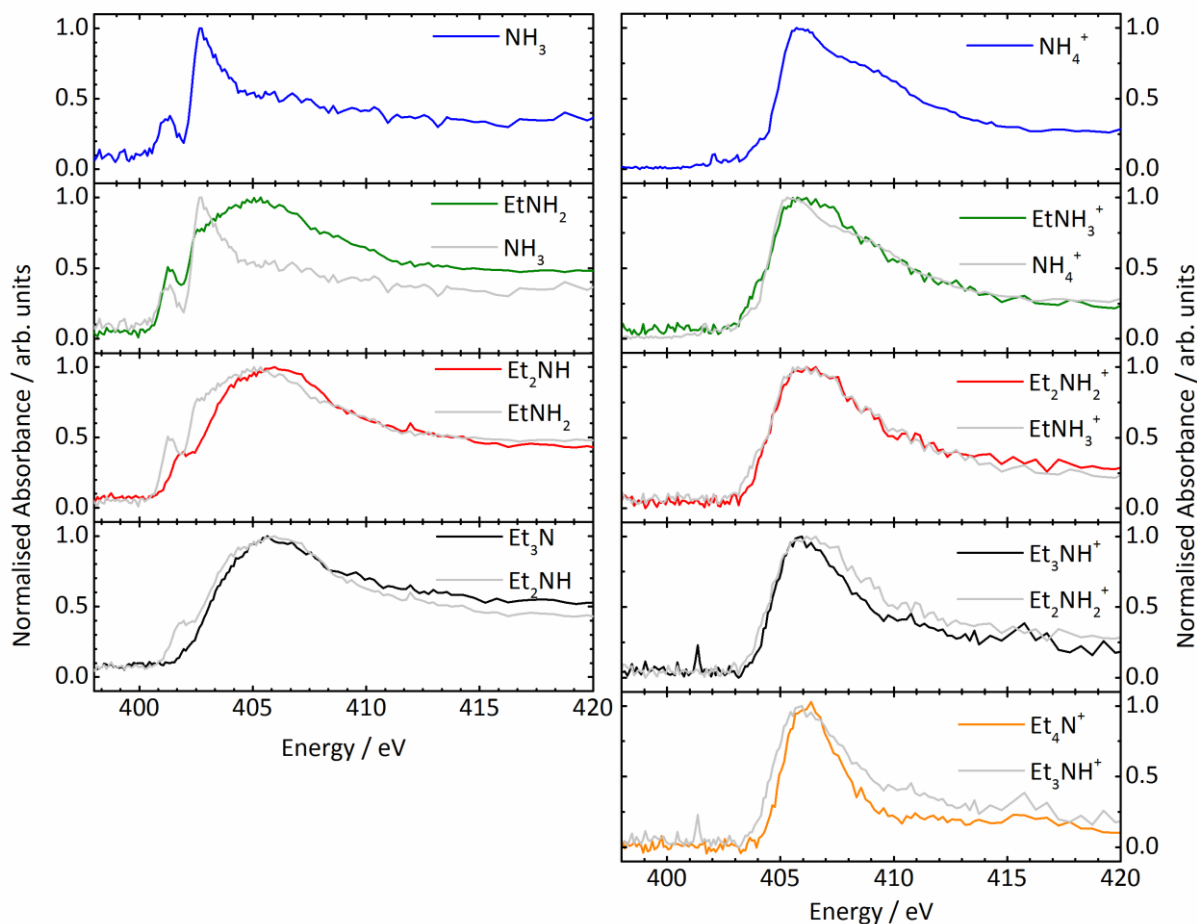


Figure 2 (left) N K-edge spectra of alkylamines $\text{Et}_x\text{NH}_{3-x}$ ($x=0..3$) in ethanol. To emphasize the changes in spectral features upon consecutive exchange of N-H for N-Et groups, for each alkylamine $\text{Et}_x\text{NH}_{3-x}$ ($x=1..3$), the spectrum of $\text{Et}_{x-1}\text{NH}_{4-x}$ ($x=1..3$) is shown as grey line in the panels as well. (right) N K-edge spectra of alkylammonium $\text{Et}_y\text{NH}_{4-y}^+$ ($y=0..4$) chloride salts in water. To emphasize the changes in spectral features upon consecutive exchange of N-H for N-Et groups, for each alkylammonium $\text{Et}_y\text{NH}_{4-y}^+$ ($y=1..4$) chloride, the spectrum of $\text{Et}_{y-1}\text{NH}_{5-y}^+$ ($y=1..4$) is shown as grey line in the panels as well.

In Figure 2 (right column) we show the experimental N K-edge absorption spectra measured for the alkylammonium $R_y\text{NH}_{4-y}^+$ ($R = \text{C}_2\text{H}_5-$ (Et-); $y=0..4$) series dissolved in water. The absorption spectrum of $\text{NH}_4^+(\text{aq})$ has been published in our previous study on $\text{NH}_3(\text{aq})/\text{NH}_4^+(\text{aq})$.⁵ We found that $\text{NH}_4^+(\text{aq})$ exhibits a strong main-edge band located at 405.7 eV, accompanied by a minor pre-edge at 403-404 eV and a significantly pronounced post-edge at about 409 eV (Figure 2). To emphasize the changes in spectral features upon consecutive exchange of N-H for N-Et groups, for each alkylammonium $\text{Et}_y\text{NH}_{4-y}^+$ ($y=1..4$), the spectrum of $\text{Et}_{(y-1)}\text{NH}_{4-(y-1)}^+$ ($y=1..4$) is shown as grey line in the panels as well. Subsequent exchange in the number of N-H groups by ethyl-groups does not lead to a significant shift in frequency positions of the observable transitions. Increasing the number of ethyl-groups leads to a further decrease in intensity of both the pre- and post-edge parts of the N K-edge spectra relative to that of the main-edge, leading to an effective apparent “narrowing” of the overall spectra.

In addition, we measured ammonia NH_3 and diethylamine Et_2NH both in water and in ethanol to investigate the influence of solute-solvent hydrogen bonding (see Figure 3). Here we note that NH_3 dissolved in ethanol has been prepared using concentrated aqueous NH_3 , which amounts to a molar ratio of $[\text{NH}_3] : [\text{H}_2\text{O}] : [\text{EtOH}] = 1 : 2.8 : 22.7$. In the measurements presented here we have not found any significant variations in the solvent-induced frequency shift in the pre- and main-edge bands, located at 401.2 eV and 402.8 eV for NH_3 , respectively. For Et_2NH a pre-edge appears around 401.7-401.9 eV whereas the main-edge has merged with the post-edge band. Whether this apparent difference in spectral position of the pre-edge of Et_2NH in EtOH compared to that in H_2O is caused by a real frequency up-shift, or the consequence of somewhat larger line broadening (in conjunction with larger spectral overlap with main-edge transitions) cannot be determined within the current

measurement accuracy. We deduce from the measurements shown in Figure 3, that the effects of hydrogen bonding and solvation on the N K-edge transitions of NH_3 and Et_2NH are similar for H_2O and ethanol. It has been shown earlier⁴ that the whole N K-edge absorption spectrum of aqueous NH_3 predominantly shifts due to the accepting hydrogen bond. We now have provided compelling evidence that the effects of hydrogen bonding and solvation are of similar magnitude in water and in ethanol, for the alkylamine compounds. Even more so, this supports our notion that we can compare not only the set of alkylamine compounds in ethanol, and that of the alkylammonium ions in water as separate series, but with N K-edge absorption spectroscopy we can also attempt to compare the alkylamine bases with the respective alkylammonium conjugate acid ions, to assess the impact of transferring a proton to the nitrogen lone pair.

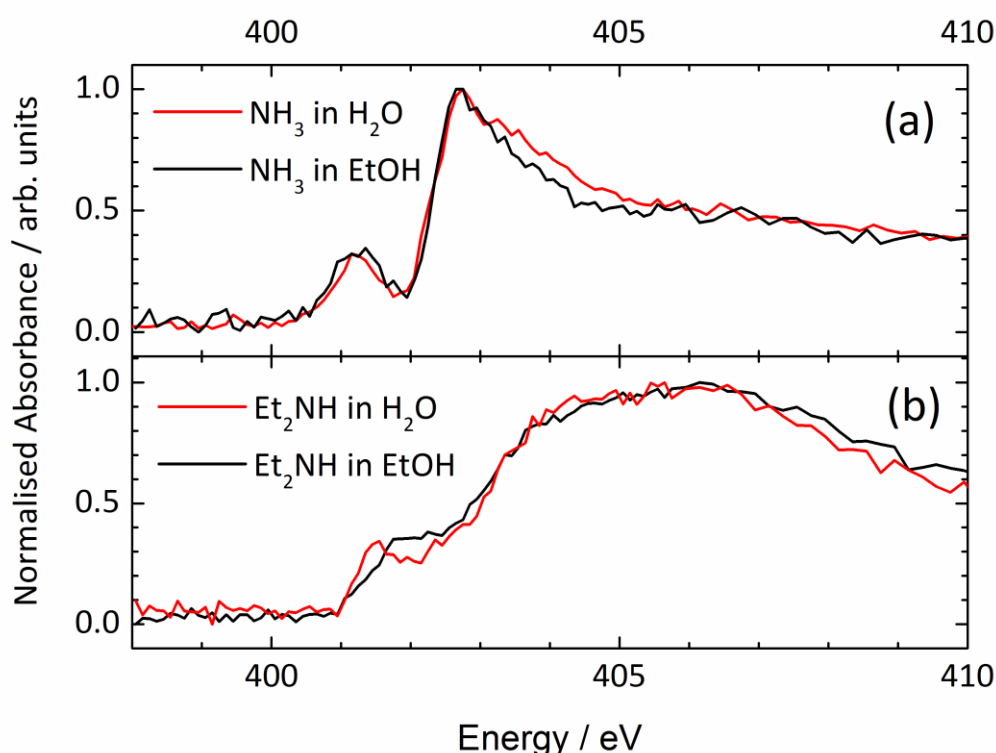


Figure 3 N K-edge spectra of (a) NH_3 and of (b) Et_2NH measured in ethanol and in water.

The main conclusion to be drawn from the N K-edge spectra of the two series of molecular systems is that the main edge transitions are at a similar frequency within each set of molecular systems (403 eV and 406 eV for the alkylamines and alkylammonium ions, respectively), and that the frequency offset between the main edge transitions of alkylamines vs. alkylammonium ions has a consistent value of 3 eV. A marked difference occurs in the consecutive exchange of the N-H functionality with N-ethyl-groups. For alkylamines an increase in the number of ethyl-groups leads to the pre-edge transition merging with the main-edge transition, and both of them ultimately disappearing underneath a major post-edge band, that should have its origin in the binding to the ethyl-groups. In contrast, for the alkylammonium ions the more ethyl-groups are present, the less pronounced both pre- and post-edge transitions are with respect to the main-edge band, with no apparent additional contributions. This main-edge band must be due to N 1s excitations to unoccupied orbitals with different character for NH_4^+ and for Et_4N^+ . Nevertheless it appears to be located at about the same transition frequency. We will attempt to explain the experimental observations and trends by quantum-chemical modelling of XAS features for the isolated and hydrogen bonded solutes.

4. Computational Results

The impact of hydrogen bonding on the O K-edge of O-H groups in protic solvents like water and alcohols has now been widely documented.^{36, 37, 38} Hydrogen bonding plays a key role in altering the cross sections of 1s excitations to lowest unoccupied orbitals, as probed with XAS, due to changes in orbital symmetries as well in electronic densities of the electronegative O atoms being changed upon by (donating or accepting) hydrogen bonding interactions. In a similar fashion hydrogen bonding will also govern the changes in the N K-edge spectral features of amino-groups. To obtain a more complete understanding of the impact of hydrogen bonding for the alkylamine and alkylammonium series studied here the N K-edge XAS spectra of hydrogen-bonded clusters are calculated for different hydrogen-bonded configurations. The role of the fluctuating solvent surrounding the solute molecules can be optimally grasped with *ab initio* molecular dynamics (AIMD) calculations. AIMD calculations, however, are costly, and beyond the objectives of the current study. Here we simulate the effects on the pre-, main- and post-edge features in the N K-edge absorption resonances, by inspection of various forms of hydrogen bonded clusters of the alkylamines and alkylammonium ions. (Alkylamines can donate hydrogen bonds through their N-H groups, and accept hydrogen bonds by the amino nitrogen lone pair.) In Table 1 we present the results of binding energy calculations for the accepting and donating hydrogen bonds in the alkylamines, that exhibit the same trend as our previous AIMD simulations of aqueous ammonia.⁵ Indeed, these results show that the accepting hydrogen bond is strong suggesting it will have a major prominence in the possible solute-solvent configurations. In contrast, the donating hydrogen bond is much weaker, and will not be energetically competing with the numerous solvent-solvent interactions to have a significant impact in the

distribution of possible hydrogen-bond configurations in solution. Hence, we conclude that whereas alkylamines form strong accepting hydrogen bonds, the presence of donating hydrogen bonds is not representative for alkylamines in water or ethanol. On the other hand, alkylammonium ions can only have donating hydrogen bonds through their respective N-H groups. Our previous AIMD simulation of aqueous ammonium and the similar magnitudes of binding energies in the present calculations summarized in Table 1 clearly show that we can expect full hydrogen bonded configurations to dominate both in water and ethanol solutions.

Table 1. Binding energies of hydrogen bonds from DFT calculations (in kJmol⁻¹)

Number of ethyl-groups (x=0..3, y=0..3)	Et _x NH _{3-x} (EtOH)	Et _x NH _{3-x} (H ₂ O)	Et _x NH _{3-x} (EtOH) _{3-x}	Et _x NH _{3-x} (H ₂ O) _{3-x}	Et _y NH _{4-y} ⁺ (H ₂ O) _{4-y}
	1 accepting hydrogen bond	1 accepting hydrogen bond	(3-x) donating hydrogen bonds ^{1,2}	(3-x) donating hydrogen bonds ^{1,2}	(4-y) donating hydrogen bonds ¹
0	-28.77	-30.42	-17.74	-8.91	-69.14
1	-37.24	-37.87	-16.53	-10.90	-64.51
2	-40.79	-40.40	-22.00	-13.84	-61.92
3	-45.93	-42.97			-60.15

¹: value per donating hydrogen bond; ²: cf. binding energies of donating hydrogen bond in (H₂O)₂ = -21.56 kJmol⁻¹ and in (EtOH)₂ = -27.14 kJmol⁻¹.

We have calculated the XAS spectra of the alkylamines Et_xNH_{3-x} (x=0..3), hydrogen-bonded to ethanol molecules and of the alkylammonium ions Et_yNH_{4-y}⁺ (y=0..4) hydrogen-bonded to water molecules, at geometries optimized through energy minimization in the electronic ground state. Figure 4 shows the comparison of the calculated N K-edge XAS of

the alkylamines (isolated $\text{Et}_x\text{NH}_{3-x}$, and hydrogen-bonded with ethanol molecules at either the donating or the accepting sides) with the experimental spectra. A good correspondence is found between the experimental spectra and the spectra of the isolated alkylamine molecules $\text{Et}_x\text{NH}_{3-x}$, in terms of frequency shifts and relative cross sections of pre-, main- and post-edge transitions. The calculated spectra clearly show that consecutive exchange of N-H with Et-N in the $\text{Et}_x\text{NH}_{3-x}$ alkylamine series leads to a relative diminishing of magnitudes of pre- and main-edge transitions with respect to those due to the increasing amount of post-edge transitions, in line with the experimental observations. We also notice the influence of hydrogen bonding on the calculated spectra. As found before for ammonia,⁴ an accepting hydrogen bond at the nitrogen lone-pair leads to a constant blue-shift of the XAS transitions. Here only minor spectral changes are observed on the accepting hydrogen bonds (red dashed lines in Figure 4). In contrast, donating hydrogen bonding involving the N-H groups significantly alters the spectra (blue dashed lines in Figure 4). In the Discussion section below, we will elaborate on the occurrence of N-H donating hydrogen bonding in the alkylamine solutions. Here, we only note that the intensity decrease of pre-edge features for the hydrogen-bonded configurations, and the associated loss of agreement of the predicted (blue dashed lines in Figure 4) with experimental spectra, is consistent with the assumption that donating hydrogen bonds around the alkylamines are minority structures in solution, as we have previously shown for aqueous ammonia.⁵ Since the accepting hydrogen bond does not influence the spectral shape and donating hydrogen bonds are likely weak or even absent, we will neglect hydrogen bonding in our assignment of the spectral features below. In Figure S1 in the Supplement, we also show the close similarity of the spectral response of the alkylamines to hydrogen bonding with ethanol and with water.

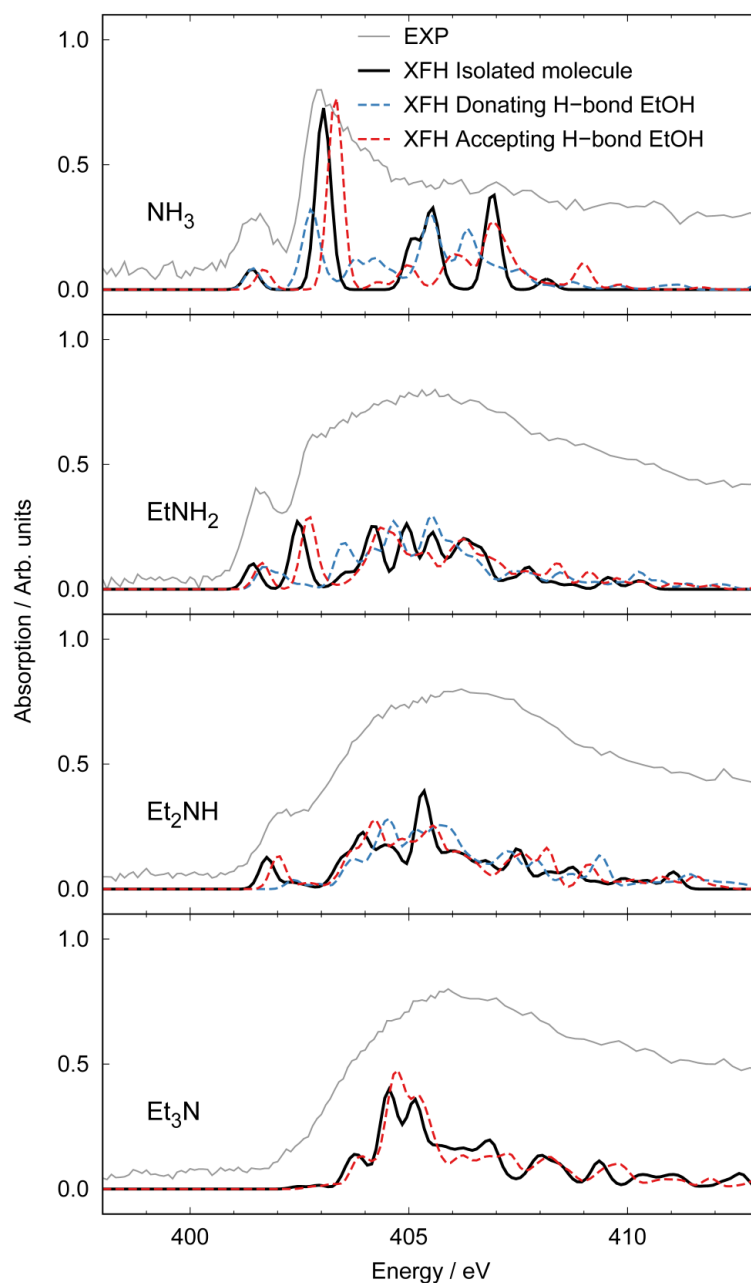


Figure 4 Simulated XA spectra of the ethylamine series using the XFH method. The vertical scales of the calculated spectra of the alkylamines are directly proportional to each other. Experimental traces, shown as grey solid lines, have an arbitrary scale; cf. left column in Figure 2. Both the isolated solutes and hydrogen bonded clusters with ethanol molecules are investigated, to determine the sensitivity to solute-solvent interactions in the first solvation shell. For the ethylamines, we consider individual accepting or donating hydrogen bond interactions.

Motivated by the limited spectral influence of accepting hydrogen bonds and by the good agreement between the experimental spectra and spectra of the isolated alkylamine molecules, we will use these models for discussing the assignment. In Figure 5 we depict the molecular orbitals associated with the dominant discrete transitions underlying the calculated XAS spectra in Figure 4. Starting with the simplest amine $\text{Et}_x\text{NH}_{3-x}$ with $x=0$, i.e. ammonia, the pre- and main-edge XAS features are associated with the 4a1 and 2e molecular orbitals as observed for aqueous ammonia^{4,5} and the N-H σ^* character of these orbitals will form the theme for understanding the trends in the N K-edge XAS of the $\text{Et}_x\text{NH}_{3-x}$ alkylamine series in ethanol. At the other end of the $\text{Et}_x\text{NH}_{3-x}$ series with $x=3$, for Et_3N the pre-edge features, associated transitions into states with N-H σ^* character, are absent and the main contributions to the spectrum are due to post-edge features, arising from a N-C σ^* shape-resonance.³⁹ In the intermediate EtNH_2 and Et_2NH molecules, the N-H σ^* features at the pre- and main-edges are systematically decreasing. Viewing the whole series from $x=0$ to $x=3$, we can observe the gradual change of the lowest unoccupied molecular orbital (LUMO) associated with the pre-edge, increasingly losing N-H σ^* character and increasingly acquiring N-C σ^* character (see Figure 6). The spectral features of transitions into states with N-C σ^* character occur in a range of higher transition frequencies and are spread over several transitions, due to hybridization with other bonds within the molecule. Thereby, we can rationalize the main spectral trends over the alkylamine series with reference to the electronic structure of the isolated solutes alone. Since the N-H groups are essentially not involved in donating hydrogen bonds to the solvent, the pre-edge features are not quenched by intermolecular interactions.

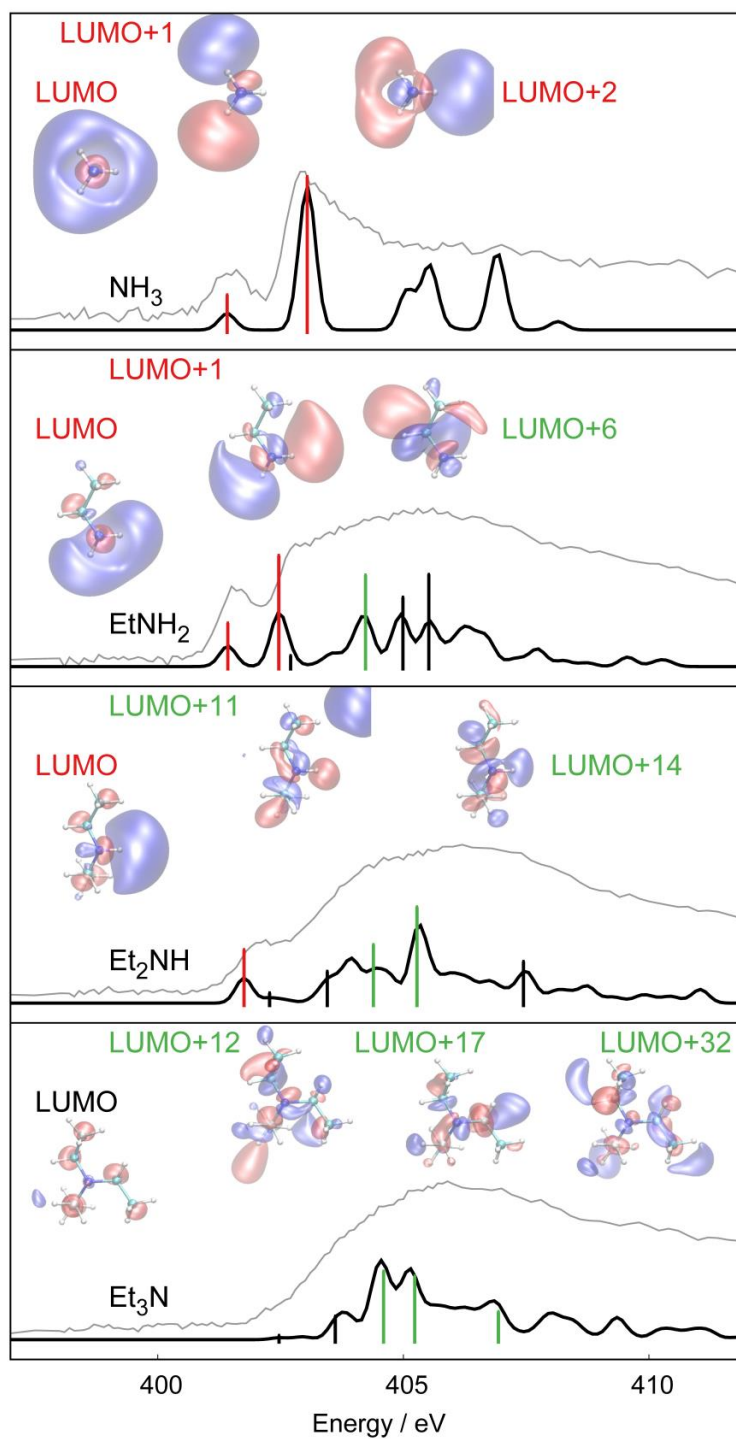


Figure 5 Molecular orbital character of the discrete XA transitions underlying the simulated XA spectra of the ethylamine series in Figure 4 (experimental traces shown as grey solid lines). Strong transitions are denoted by sticks, which are colored according to dominant final state N-H σ^* character (in red) or dominant final state C-N σ^* character (in green).

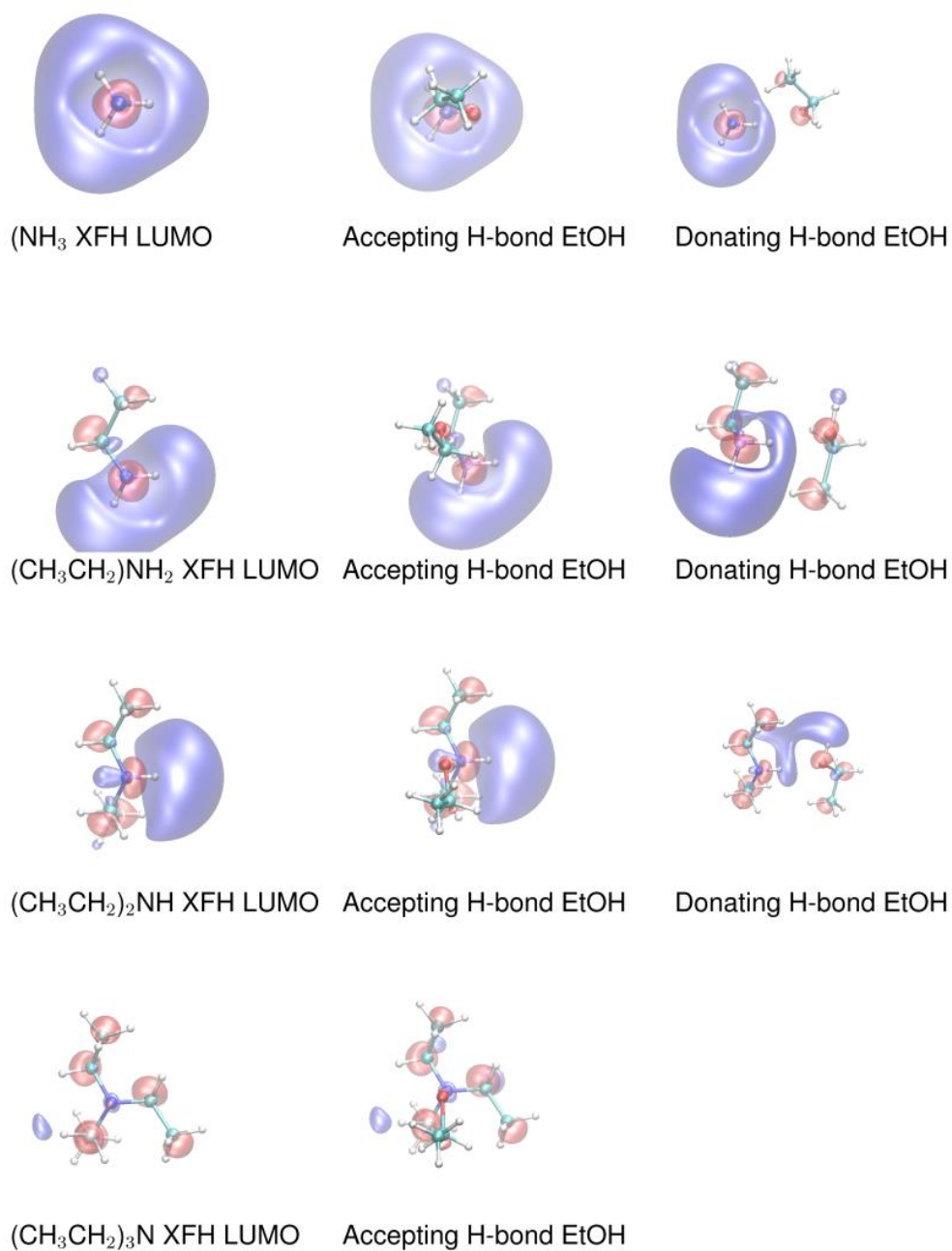


Figure 6 LUMO orbitals of the XA spectrum of Et_xNH_{3-x} (x=0..3) and the influence of hydrogen bonding.

Figure 7 shows the calculated N K-edge XAS of the alkylammonium ions for both the isolated $\text{Et}_y\text{NH}_{4-y}^+$ and the full hydrogen-bonded case $\text{Et}_y\text{NH}_{4-y}^+(\text{H}_2\text{O})_{4-y}$ (here to water molecules). We first analyze the spectra of the free cations (without hydrogen bonds). Due to near tetrahedral symmetry of the calculated alkylammonium ion clusters the pre-edge transition has close to zero transition dipole moment (i.e. absorption intensity). For ammonium and tetraethylammonium ions, the XAS spectra consist of single dominant peak from a three-fold nearly degenerate state with N-H σ^* or N-C σ^* character, respectively. For the other alkylammonium ions in the series, the symmetry breaking results in weakly allowed pre-edge features. The calculated main-edge transition(s) are not located at exactly the same frequency position as the experimental spectra seem to imply. For the alkylammonium series, we observe a shift in the main resonance, in disagreement with experiment. We speculate that this is associated with a polarization of the solvent, which is not taken into account in our models. A strong post-edge contribution located at a small frequency range is replaced by a larger number of transitions extending over a broader frequency range for an increasing number of ethyl-groups. The experimentally observed spectral transformation from a single broad feature in Et_4N^+ to pronounced main-edge and post-edge features in NH_4^+ can only be explained, if we take solvation into account. As seen for the full hydrogen bonded configurations in Figure 8, hydrogen bond donation makes the contribution from the N-H bonds split into two spectral features at approximately 406 eV (denoted by red sticks and associated with final states of N-H σ^* character) and 408 eV (denoted by blue sticks and associated with final states of N-H \cdots O σ^* character). The intensity of the high-energy feature decreases systematically with increasing number of ethyl-groups. Note that we do not describe the spectral shape of the aqueous ammonium XAS spectrum well, neither in our cluster models here nor in our previous sampling from AIMD simulations.

However, the observed splitting seems to be essential for understanding the presence of both main-edge and post-edge features for aqueous ammonium. Exchanging N-H groups by alkyl-groups in the hydrogen-bonded configurations entails a reduction of the splitting of these two main transitions and an increase of the peak at lower energies until, in Et_4N^+ , only the lower-energy peak is left. This explains the experimentally observed narrowing of the absorption band (the blue shift remains unexplained). The orbital analysis of the full hydrogen bonded cations presented in Figure 8 clearly shows that the broad alkylammonium XAS spectra consist of a main-edge of N-H σ^* and N-C σ^* final state character and a post-edge with N-H \cdots O σ^* final state character. Over the series, we can see a gradual decrease of the post-edge resonance, whereas at the main-edge the N-H σ^* and N-C σ^* features nearly coincide in energy. The intensities of the N-H σ^* and N-H \cdots O σ^* contributions depend strongly on the strength of hydrogen bonding, and these are difficult to determine accurately without sampling over different configurations using explicit solvation models.

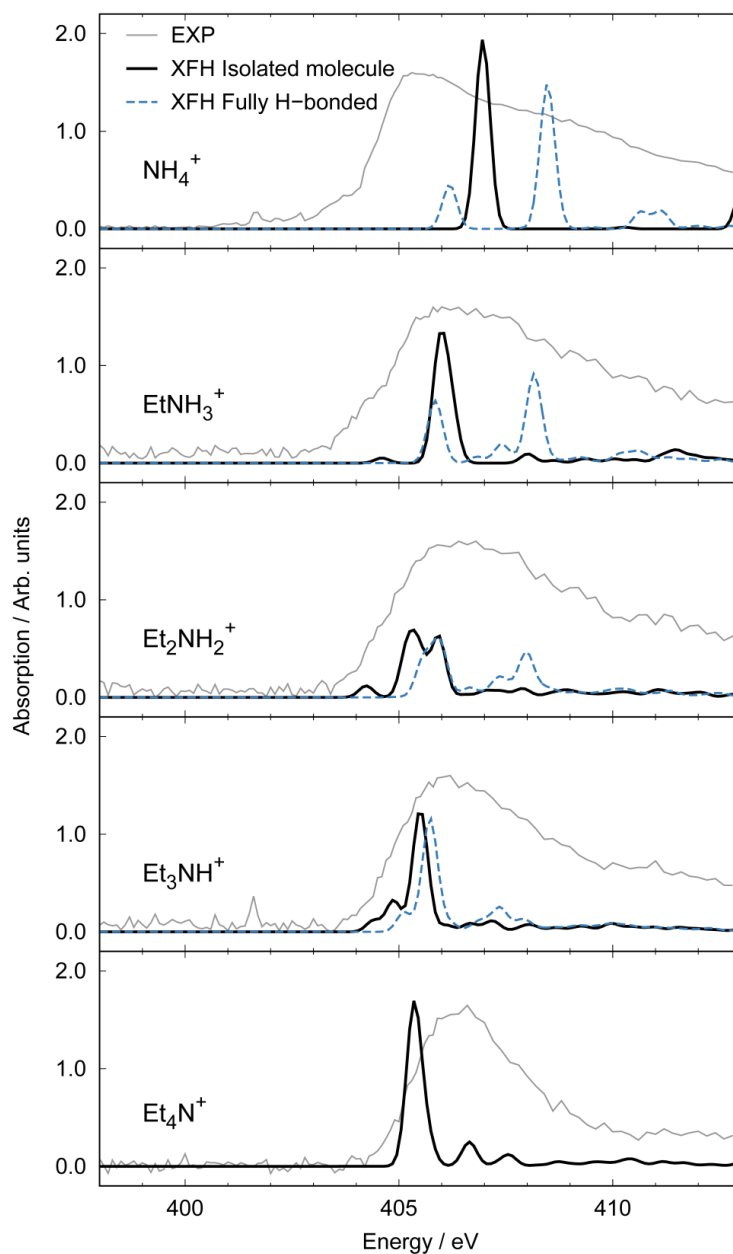


Figure 7 Simulated XA spectra of the ethylammonium ion series using the XFH method. The vertical scales of the calculated spectra of the alkylammonium ions are directly proportional to each other. shown as grey solid lines, have an arbitrary scale; cf. right column in Figure 2). Both the isolated solutes and hydrogen bonded clusters are investigated, to determine the sensitivity to solute-solvent interactions in the first solvation shell. For the alkylammonium ions, only the full hydrogen bonded cluster case is shown here.

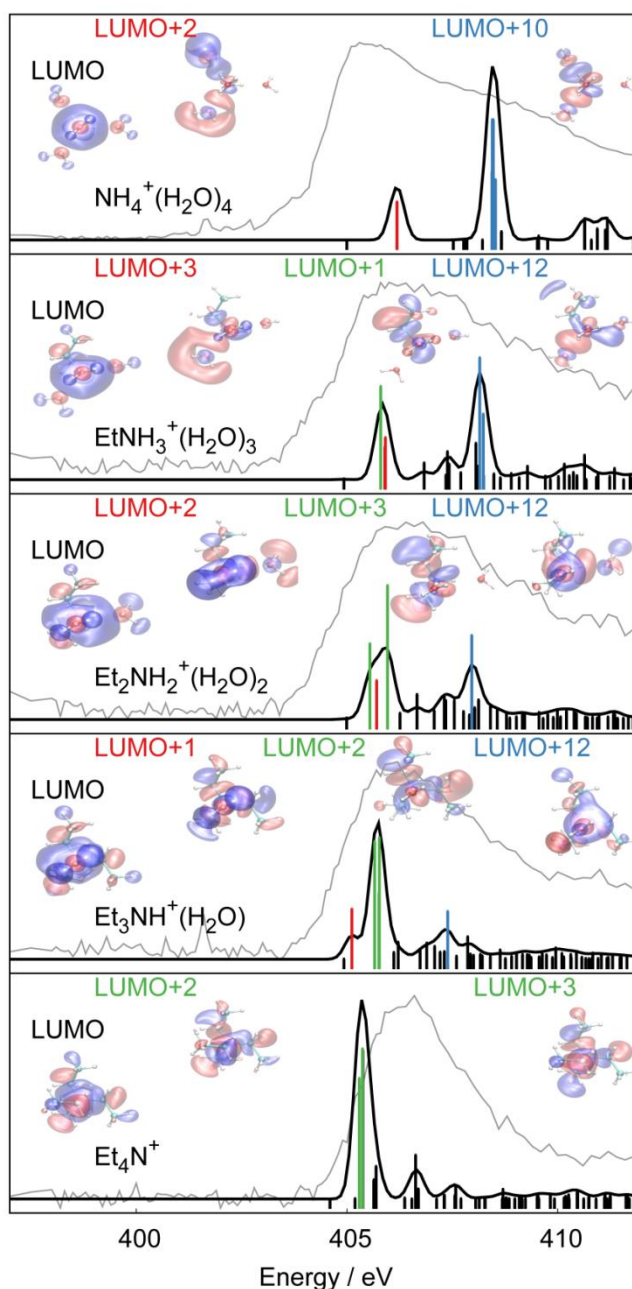


Figure 8 Molecular orbital character of the discrete XA transitions underlying the simulated XA spectra of the ethylammonium series in Figure 6. Strong transitions are denoted by sticks, which are colored according to dominant final state N-H σ^* character (in red), dominant final state C-N σ^* character (in green), or dominant final state $\sigma^*(\text{H-bond})$ character (in blue).

5. Discussion

In our previous study on aqueous $\text{NH}_3/\text{NH}_4^+$ we have described how the N K-edge spectral contributions of $\text{NH}_4^+(\text{aq})$ and of $\text{NH}_3(\text{aq})$ can be ascribed to N 1s excitations to particular unoccupied orbitals and how the electronic structure and molecular symmetry play a role in these excitations. To further discuss our observations on the N K-edge spectral features of the alkylammonium ions/alkylamines we follow a similar line of argument, based on the unoccupied orbital structure for pyramidal or tetrahedral geometries as reported before.^{37,}

³⁹ The changes in intensity of the pre-edge peaks in the series of alkylamines can be understood by inspecting the symmetries of the unoccupied orbitals reached in the XAS transitions. With C_{3v} molecular symmetry in NH_3 , the LUMO has a1 symmetry with considerable N 2p character (see the depicted molecular orbitals in Figure 5). As a result the pre-edge transition to the LUMO has substantial cross section, about one third of the cross section of the main-edge transition associated with the double degenerate LUMO+1 orbital (with e symmetry).^{37, 39} For NH_4^+ in perfect tetrahedral symmetry, in a similar fashion as for isoelectronic CH_4 , the 1s to LUMO transition is dipole forbidden due to the LUMO a1 symmetry (i.e. pure 2s character without 2p admixture). Instead the 1s to LUMO+1 transition in NH_4^+ is strongly allowed due to the exclusive 2p character of the triply degenerate LUMO+1 state (of t_2 symmetry). Hydrogen bonding interactions can induce changes in symmetry in molecular and electronic structure and thus affect the relative intensities of these transitions. For $\text{NH}_3(\text{aq})$ the effects of hydrogen bonding are moderate, as the hydrogen bond donating capacity of the N-H groups is too small to be of importance, and only the hydrogen bond accepting by the nitrogen lone pair with one water molecule is to be considered. Because the LUMO and LUMO+1 orbitals remain to a large extent localized on the NH_3 molecule, when embedded in water, hydrogen bonding effects are not

significantly altering the pre- and main-edge transitions at the N K-edge. Instead, the post-edge transition increases in intensity due to the hybridization of the unoccupied orbitals of NH_3 with the water molecule hydrogen bonded to the nitrogen lone pair. In the case of $\text{NH}_4^+(\text{aq})$ – dominated by hydrogen bond donating interactions with four water molecules and on average only few uncoordinated N-H groups – hydrogen bond effects are larger, by either frequency shifts (caused by a distribution in absorption transition frequencies), symmetry breaking (e.g. making the pre-edge transition increase in cross section), or by hybridization to the solvent shell water molecules (clearly pronounced for the post edge band). We note in particular the presence of a shape resonance associated with hydrogen bonding for the protonated alkylammonium systems.

Binding energies of the hydrogen bonds between solute and solvent molecules as estimated from the optimization in DFT calculations do change in the alkylamine and alkylammonium ion series, and differ when having either water or ethanol as hydrogen bond partners (see Table 1). We can draw the following conclusions from these binding energy calculations: 1) The accepting hydrogen bond of the ethylamines is of comparable strength in ethanol and in water. 2) The donating hydrogen bond of the ethylamines is significantly weaker than the accepting hydrogen bond in both solvents. 3) The donating hydrogen bond of the ethylamines is significantly stronger in ethanol than in water. 4) The accepting hydrogen bond of the ethylamines gradually increases in strength with increasing number of ethyl-groups. 5) The donating hydrogen bond of the ethylamines gradually increases in strength with increasing number of ethyl-groups. 6) The donating hydrogen bond of the ethylammonium ions is strong but gradually decreases in strength with increasing number of ethyl-groups. However, we also note that hydrogen bonding is stronger in the ethanol dimer

than in the water dimer. Hence, it is difficult to estimate whether hydrogen bonds of the ethylamines donating to the ethanol solvent actually are strong enough to compete with those amongst ethanol molecules and are truly identifiable as significant solute-solvent interaction. Likewise, we can only point out the indication that the number of donating hydrogen bonds around ethylammonium might decrease with increasing number of ethyl-groups, based on both steric and energetic arguments.

Based on these computational results it is clear that the medium strong accepting hydrogen bond between the nitrogen lone pair and one solvent molecule is the dominating hydrogen bond interaction for NH_3 . The hydrogen bond donating interactions are only half as strong (per N-H group) and cannot compete with the solvent-solvent interactions. Figure 3 shows that the N K-edge spectra of NH_3 dissolved in ethanol and in water are similar within measurement accuracy, implying that any possible differences in hydrogen bond interactions of NH_3 with these two protic solvents are not reflected in significant changes in the XAS spectral features. We conclude that solvent-dependent differences in the N K-edge spectral features – such as spectral shifts or relative intensity changes of pre-, main- or post-edges – are definitely smaller than the observed line broadening when discussing ethanol and water as solvents. We note that for the ethylamine series similar medium strong accepting hydrogen bond interactions exist in both solvents, and the same donating hydrogen bond interactions (per N-H group) at about twice the magnitude when comparing ethanol and water. Hence we argue that our observations obtained in the XAS of ethylamines in ethanol can also be expected to occur in aqueous solution. A similar argument can be used for the ethylammonium ions, where the hydrogen bond donating interactions only change up to 13 % (per N-H group) when going from NH_4^+ to Et_3NH^+ .

For a closer inspection of the unoccupied orbitals reached by the N 1s excitations, we can follow the line of argument as used in the study on $\text{NH}_3(\text{aq}) / \text{NH}_4^+(\text{aq})$.⁵ Eventhough a partial exchange of N-H groups with ethyl-groups leads to a formal symmetry breaking, from an electronic structural point of view the ethylamines maintain a pyramidal geometry, and the ethylammonium ions can be considered as having a tetrahedral configuration. Despite maintaining either a pyramidal or tetrahedral geometry, a consecutive change of N-H bonds for N-ethyl-groups may change the nature of the unoccupied orbitals reached (with associated changes in transition dipole moments), and will change the effects caused by hydrogen bonding interactions.

6. Conclusions

In our combined experimental and computational study of the N K-edge absorption spectroscopy of the acid-base ethylammonium ion/ethylamine pairs, we can explain the systematic changes in spectral features upon consecutive exchange of N-H groups with ethyl-groups. To understand the observations we have argued that an effective pyramidal electronic structure locally at the central N-atom prevails for the entire ethylamines $\text{Et}_x\text{NH}_{3-x}$ ($x=0..3$) series. In a similar way a tetrahedral electronic structure at the N-atom can be used to explain the results obtained on the ethylammonium ion $\text{Et}_y\text{NH}_{4-y}^+$ ($y=0..4$) series. More unoccupied orbitals can be reached upon N 1s core excitation with an increasing number of ethyl-groups. These unoccupied orbitals have a varying N-H σ^* to N-C σ^* final state character. For the ethylamines measured in ethanol solution, the pronounced pre- and main-edge transitions predominantly have N-H σ^* characteristics, that are quenched with an

increasing number of ethyl-groups, and ultimately disappear under the larger number of transitions observed over a broader frequency range extending well into the post-edge, that can be associated with excitations to unoccupied orbitals with N-C σ^* final state character. For the ethylammonium ion series, measured in aqueous solution, pre- and post-edge transitions with predominantly N-H σ^* and N-H \cdots O σ^* final state character observed for NH_4^+ diminish in magnitude upon consecutive exchange of N-H by N-Et groups, and ultimately a strong main-edge band, having C-N σ^* final state character, fully dominates the N K-edge spectrum for Et_4N^+ . Despite the fact that the unoccupied orbitals reached at the main-edge energies acquire a significantly different character with increasing number of ethyl-groups, no significant shifts are observed experimentally.

In this study, we have shown that the essence of the experimental XAS of the series of alkylamines in ethanol and alkylammonium ions in water can be captured in simple cluster models. Although the simulated spectra reproduce the main spectral features and trends, discrepancies found when making a detailed comparison require further investigations using more realistic models, including dynamical sampling and long-range interactions.⁵ This modeling at advanced levels will allow for a critical assessment of the quantitative predictability of the spectra with theoretical methods. Nevertheless, our findings on the N K-edge spectroscopy of amino-groups, subject to the systematic change of chemical functional groups, will serve as benchmark in future studies of amine compounds, in bulk solution, as well as in biological surroundings and on interfacial systems.

Supporting Information

Simulated XA spectra of the ethylamine series using the XFH method, of ethylamines hydrogen-bonded with water molecules.

Acknowledgement

M. Ekimova and E.T.J. Nibbering acknowledge support from the German Science Foundation (Project Nr. DFG - NI 492/11-1). M. Odelius acknowledges support from the Swedish Research Council (VR contract number 2015-03956) and the Helmholtz Virtual Institute VI419 “Dynamic Pathways in Multidimensional Landscapes”. The calculations were performed on resources provided by the Swedish National Infrastructure for Computing (SNIC). Ph. Wernet and M. Kubin acknowledge financial support from the Human Frontiers Science Program (RGP0063/2013). M. Ochmann and N. Huse gratefully acknowledge funding from the Deutsche Forschungsgemeinschaft within the Sonderforschungsbereich 925 (project A4). We all greatly acknowledge the support of the BESSYII staff during x-ray measurements at the UE52_SGM Undulator SGM variable polarisation beamline of the Helmholtz-Zentrum Berlin and we thank Helmholtz-Zentrum Berlin for the allocation of synchrotron radiation beamtime.

References

1. Mannich, C. Über ein Kondensationsprodukt aus Formaldehyd, Ammoniak und Antipyrin. *Arch. Pharm.* **1912**, *205*, 647-667.
2. Blicke, F. F. The Mannich Reaction. In *Organic Reactions*, Adams, R., Ed. John Wiley & Sons: New York, 1942; Vol. 1, pp 303-341.
3. Patai, S. *The Chemistry of the Amino Group*. John Wiley & Sons: New York, 1968.
4. Weinhardt, L.; Ertan, E.; Iannuzzi, M.; Weigand, M.; Fuchs, O.; Bär, M.; Blum, M.; Denlinger, J. D.; Yang, W.; Umbach, E.; et al. Probing Hydrogen Bonding Orbitals: Resonant Inelastic Soft X-Ray Scattering of Aqueous NH₃. *Phys. Chem. Chem. Phys.* **2015**, *17*, 27145-27153.
5. Ekimova, M.; Quevedo, W.; Szyc, Ł.; Iannuzzi, M.; Wernet, P.; Odelius, M.; Nibbering, E. T. J. Aqueous Solvation of Ammonia and Ammonium: Probing Hydrogen Bond Motifs with FT-IR and Soft-X-Ray Spectroscopy. *J. Am. Chem. Soc.* **2017**, *139*, 12773–12783.
6. Messer, B. M.; Cappa, C. D.; Smith, J. D.; Wilson, K. R.; Gilles, M. K.; Cohen, R. C.; Saykally, R. J. pH Dependence of the Electronic Structure of Glycine. *J. Phys. Chem. B* **2005**, *109*, 5375-5382.
7. Otero, E.; Urquhart, S. G. Nitrogen 1s Near-Edge X-Ray Absorption Fine Structure Spectroscopy of Amino Acids: Resolving Zwitterionic Effects. *J. Phys. Chem. A* **2006**, *110*, 12121-12128.
8. Meyer, F.; Blum, M.; Benkert, A.; Hauschild, D.; Nagarajan, S.; Wilks, R. G.; Andersson, J.; Yang, W.; Zharnikov, M.; Baer, M.; et al. "Building Block Picture" of the Electronic Structure of Aqueous Cysteine Derived from Resonant Inelastic Soft X-Ray Scattering. *J. Phys. Chem. B* **2014**, *118*, 13142-13150.

9. Unger, I.; Hollas, D.; Seidel, R.; Thürmer, S.; Aziz, E. F.; Slaviček, P.; Winter, B. Control of X-Ray Induced Electron and Nuclear Dynamics in Ammonia and Glycine Aqueous Solution via Hydrogen Bonding. *J. Phys. Chem. B* **2015**, *119*, 10750-10759.
10. Meyer, F.; Blum, M.; Benkert, A.; Hauschild, D.; Jeyachandran, Y. L.; Wilks, R. G.; Yang, W.; Baer, M.; Heske, C.; Reinert, F.; et al. X-Ray Emission Spectroscopy of Proteinogenic Amino Acids at All Relevant Absorption Edges. *J. Phys. Chem. B* **2017**, *121*, 6549-6556.
11. Eckert, S.; Norell, J.; Miedema, P. S.; Beye, M.; Fondell, M.; Quevedo, W.; Kennedy, B.; Hantschmann, M.; Pietzsch, A.; Van Kuiken, B. E.; et al. Ultrafast Independent N-H and N-C Bond Deformation Investigated with Resonant Inelastic X-Ray Scattering. *Angew. Chem. Int. Ed.* **2017**, *56*, 6088-6092.
12. Prémont-Schwarz, M.; Schreck, S.; Iannuzzi, M.; Nibbering, E. T. J.; Odellius, M.; Wernet, Ph. Correlating Infrared and X-Ray Absorption Energies for Molecular-Level Insight into Hydrogen Bond Making and Breaking in Solution. *J. Phys. Chem. B* **2015**, *119*, 8115-8124.
13. Eckert, S.; Miedema, P. S.; Quevedo, W.; O'Conneide, B.; Fondell, M.; Beye, M.; Pietzsch, A.; Ross, M.; Khalil, M.; Föhlisch, A. Molecular Structures and Protonation State of 2-Mercaptopyridine in Aqueous Solution. *Chem. Phys. Lett.* **2016**, *647*, 103-106.
14. Meyer, F.; Blum, M.; Benkert, A.; Hauschild, D.; Jeyachandran, Y. L.; Wilks, R. G.; Yang, W.; Bär, M.; Reinert, F.; Heske, C.; et al. Site-Specific Electronic Structure of Imidazole and Imidazolium in Aqueous Solutions. *Phys. Chem. Chem. Phys.* **2018**, *20*, 8302-8310.
15. Fogarty, R. M.; Matthews, R. P.; Clough, M. T.; Ashworth, C. R.; Brandt-Talbot, A.; Corbett, P. J.; Palgrave, R. G.; Bourne, R. A.; Chamberlain, T. W.; Vander Hoogerstraete, T.;

et al. NEXAFS Spectroscopy of Ionic Liquids: Experiments versus Calculations. *Phys. Chem. Chem. Phys.* **2017**, *19*, 31156-31167.

16. Kelly, D. N.; Schwartz, C. P.; Uejio, J. S.; Duffin, A. M.; England, A. H.; Saykally, R. J. Communication: Near Edge X-Ray Absorption Fine Structure Spectroscopy of Aqueous Adenosine Triphosphate at the Carbon and Nitrogen K-Edges. *J. Chem. Phys.* **2010**, *133*, 101103.

17. Ekimova, M.; Quevedo, W.; Faubel, M.; Wernet, P.; Nibbering, E. T. J. A Liquid Flatjet System for Solution Phase Soft-X-Ray Spectroscopy. *Struct. Dynam.* **2015**, *2*, 054301.

18. Miedema, P. S.; Quevedo, W.; Fondell, M. The Variable Polarization Undulator Beamline UE52 SGM at BESSY II. *Journal of Large-Scale Research Facilities JLSRF* **2016**, *2*, A70.

19. Lippert, G.; Hutter, J.; Parrinello, M. A Hybrid Gaussian and Plane Wave Density Functional Scheme. *Mol. Phys.* **1997**, *92*, 477-487.

20. VandeVondele, J.; Krack, M.; Mohamed, F.; Parrinello, M.; Chassaing, T.; Hutter, J. Quickstep: Fast and Accurate Density Functional Calculations using a Mixed Gaussian and Plane Waves Approach. *Comput. Phys. Commun.* **2005**, *167*, 103-128.

21. Hutter, J.; Iannuzzi, M.; Schiffmann, F.; VandeVondele, J. CP2K: Atomistic Simulations of Condensed Matter Systems. *Wiley Interdisc. Rev. Comput. Mol. Sci.* **2014**, *4*, 15-25.

22. CP2K. *Version 5.0 the CP2K Developers Group*, <http://www.cpmc.org>. 2017.

23. Becke, A. D. Density-Functional Exchange-Energy Approximation with Correct Asymptotic-Behavior. *Phys. Rev. A* **1988**, *38*, 3098-3100.

24. Lee, C. T.; Yang, W. T.; Parr, R. G. Development of the Colle-Salvetti Correlation-Energy Formula into a Functional of the Electron-Density. *Phys. Rev. B* **1988**, *37*, 785-789.

25. Grimme, S.; Antony, J.; Ehrlich, S.; Krieg, H. A Consistent and Accurate Ab Initio Parametrization of Density Functional Dispersion Correction (DFT-D) for the 94 Elements H-Pu. *J. Chem. Phys.* **2010**, *132* (15), 154104.
26. Grimme, S.; Ehrlich, S.; Goerigk, L. Effect of the Damping Function in Dispersion Corrected Density Functional Theory. *J. Comput. Chem.* **2011**, *32*, 1456-1465.
27. Martyna, G. J.; Tuckerman, M. E. A Reciprocal Space Based Method for Treating Long Range Interactions in Ab Initio and Force-Field-Based Calculations in Clusters. *J. Chem. Phys.* **1999**, *110*, 2810-2821.
28. Krack, M. Pseudopotentials for H to Kr Optimized for Gradient-Corrected Exchange-Correlation Functionals. *Theor. Chem. Acc.* **2005**, *114*, 145-152.
29. Goedecker, S.; Teter, M.; Hutter, J. Separable Dual-Space Gaussian Pseudopotentials. *Phys. Rev. B* **1996**, *54*, 1703-1710.
30. Hartwigsen, C.; Goedecker, S.; Hutter, J. Relativistic Separable Dual-Space Gaussian Pseudopotentials from H to Rn. *Phys. Rev. B* **1998**, *58*, 3641-3662.
31. VandeVondele, J.; Hutter, J. Gaussian Basis Sets for Accurate Calculations on Molecular Systems in Gas and Condensed Phases. *J. Chem. Phys.* **2007**, *127*, 114105.
32. Prendergast, D.; Galli, G. X-Ray Absorption Spectra of Water from First Principles Calculations. *Phys. Rev. Lett.* **2006**, *96*, 215502.
33. Iannuzzi, M.; Hutter, J. Inner-Shell Spectroscopy by the Gaussian and Augmented Plane Wave Method. *Phys. Chem. Chem. Phys.* **2007**, *9*, 1599-1610.
34. Krishnan, R.; Binkley, J. S.; Seeger, R.; Pople, J. A. Self-Consistent Molecular-Orbital Methods .20. Basis Set for Correlated Wave-Functions. *J. Chem. Phys.* **1980**, *72*, 650-654.
35. Frisch, M. J.; Pople, J. A.; Binkley, J. S. Self-Consistent Molecular-Orbital Methods .25. Supplementary Functions for Gaussian-Basis Sets. *J. Chem. Phys.* **1984**, *80*, 3265-3269.

36. Wernet, Ph.; Nordlund, D.; Bergmann, U.; Cavalleri, M.; Odelius, M.; Ogasawara, H.; Näslund, L. Å.; Hirsch, T. K.; Ojamäe, L.; Glatzel, P.; et al. The Structure of the First Coordination Shell in Liquid Water. *Science* **2004**, *304*, 995-999.
37. Nilsson, A.; Nordlund, D.; Waluyo, I.; Huang, N.; Ogasawara, H.; Kaya, S.; Bergmann, U.; Näslund, L.-Å.; Öström, H.; Wernet, Ph.; et al. X-Ray Absorption Spectroscopy and X-Ray Raman Scattering of Water and Ice; an Experimental View. *J. Electron. Spectrosc. Relat. Phenom.* **2010**, *177*, 99-129.
38. Fransson, T.; Harada, Y.; Kosugi, N.; Besley, N. A.; Winter, B.; Rehr, J. J.; Pettersson, L. G. M.; Nilsson, A. X-Ray and Electron Spectroscopy of Water. *Chem. Rev.* **2016**, *116*, 7551-7569.
39. Stöhr, J. *NEXAFS Spectroscopy*. Springer: Berlin, 1996.

TOC Graphic

